Letter

Crosstalk between magnetostriction and magnetoelectric coupling in type-II multiferroic $TbFeO_3$

A. Indra [1,*] S. Mukherjee,[1] K. Dey,[1,†] O. Fabelo [2] L. Canadillas-Delgado [2]
T. Chatterji,[2] J. Strempfer,[3,‡] S. Majumdar,[1] and S. Giri[1,§]

[1]*School of Physical Sciences, Indian Association for the Cultivation of Science, Jadavpur, Kolkata 700032, India*
[2]*Institut Laue-Langevin, 71 Avenue des Martyrs, CS 20156, 38042 Grenoble Cedex 9, France*
[3]*Deutsches Elektronen-Synchrotron DESY, Notkestrasse 85, D-22607 Hamburg, Germany*

(Received 24 July 2024; revised 21 February 2025; accepted 24 March 2025; published 24 April 2025)

Laminated composites show great promise for achieving substantial magnetoelectric (ME) coupling through the manipulation of magnetostriction and piezoelectric engineering. However, the ME coupling mechanism in composites is less understood due to complex extrinsic effects at the interfaces, unlike the well-understood ME mechanism in chemically single-phase compounds. Our study reveals unexplored ferroelectric (FE) orders along *c*-axis and magnetostriction-driven ME couplings, indicating type-II multiferroic order in $TbFeO_3$ and providing insight into the controversy surrounding ferroelectricity in $RFeO_3$ orthoferrites. Neutron and synchrotron x-ray diffraction (SXD) results indicate exchange striction-driven FE order below 200 K, with Tb order leading to ferroelectricity below 3 K. SXD results also reveal significant magnetostriction along the *c*-axis, correlating with ME coupling at both FE orders. These findings directly demonstrate magnetostriction-driven ME coupling, and they suggest it as one of the potential mechanisms underlying ME coupling in multiferroics.

DOI: 10.1103/PhysRevB.111.L140412

The magnetoelectric (ME) effect, which signifies the induction of electric polarization due to a magnetic field and magnetization induced by an electric field, was initially demonstrated by Röntgen in 1888 [1] and was first hypothesized by Curie in 1894 [2]. The ME coupling has regained significance as researchers delve into its implications in multiferroics [3–5], thereby renewing interest in this cross-coupling phenomenon. In particular, the intrinsic coupling between electric and magnetic orders [6–10] in multiferroics has evoked intensive interest, given its potential applications in spintronics [11,12], magnetic data storage devices [8–10,13], memory applications [14,15], and even for biomedical applications [16]. Beyond fundamental interest, the potential applications in multiferroics have motivated the research community to explore new multiferroics, where significant ME coupling coincides with a substantial ferroelectric polarization (P) close to room temperature. Unfortunately, the ME coupling has been reported to be weak and/or realized far below room temperature in most of these multiferroics, with very few exceptions, such as $BiFeO_3$ [17,18], CuO [19], and $Sr_3Co_2Fe_{24}O_{41}$ [20]. While the ME coupling is weak, $BiFeO_3$ stands out as the most celebrated type-I multiferroic system, boasting a considerable P-value and multiferroic order well above room temperature [17,18]. In the case of CuO, ferroelectric order was observed within a limited temperature range of 213–230 K [19]. The compound, $Sr_3Co_2Fe_{24}O_{41}$ exhibited ferroelectric order above room temperature [20]. However, its P-value is not as promising, limited to $\sim 30\ \mu C/m^2$. High-temperature ferroelectric order and significant magnetoelectric coupling have been explored in only a few compounds, such as $YBaCuFeO_5$ [21], $Bi_{4.2}K_{0.8}Fe_2O_{9+\delta}$ [22], γ-$BaFe_2O_4$ [23]. Consequently, identifying promising multiferroics remains a challenging issue.

In recent times, there has been a notable surge in interest surrounding rare-earth orthoferrites, $RFeO_3$ (R denotes rare earth), due to their intricate and diverse magnetic properties [24–26] and the recent revelation of multiferroic order across a broad temperature spectrum, ranging from near room temperature to the frigid temperatures close to that of liquid helium temperature [6,27–31].

The $RFeO_3$ compounds crystallize in the orthorhombic $Pbnm$ space group and comprise two different magnetic ions: the $4f$ R^{3+} and the $3d$ Fe^{3+} ions. Consequently, three types of magnetic interactions emerge—Fe^{3+}-Fe^{3+}, Fe^{3+}-R^{3+}, and R^{3+}-R^{3+}—leading to the complex and interesting magnetic properties in $RFeO_3$. Typically, in the majority of $RFeO_3$ compounds, the Fe^{3+} ions exhibit ordering at higher Néel temperatures (T_N) within the range of 620–740 K, adopting a G-type canted antiferromagnetic (AFM) structure. This results in the manifestation of weak ferromagnetism (FM). Below T_N, the magnetic structure undergoes a gradual spin reorientation transition due to $3d-4f$ interactions, occurring as the material cools through a specific temperature range [32,33]. Eventually, R^{3+} orders below 10 K. Interestingly, recent studies have revealed that the $3d-4f$ interaction may play a crucial role in the emergence of multiferroic as well as ME properties in $RFeO_3$ compounds. For instance, the

*Present address: Department of Physics, Srikrishna College, Bagula, Nadia, West Bengal 741502, India.
†Present address: Department of Physics, SBSS Mahavidyalaya, Goaltore, Paschim Medinipur, West Bengal 721128, India.
‡Present address: Advanced Photon Source, Argonne National Laboratory, Lemont, Illinois 60439, USA.
§Contact author: sspsg2@iacs.res.in

exchange interaction between R^{3+} and Fe^{3+} spins results in a substantial ferroelectric (FE) polarization along the c-axis in $GdFeO_3$ [27,34,35] and $DyFeO_3$ [30]. However, these FE orders occur below the R^{3+} ordering at 2.5 and 3.5 K for $GdFeO_3$ and $DyFeO_3$, respectively. In contrast, ferroelectricity near room temperature was observed in epitaxially grown $YbFeO_3$ [36], $GaFeO_3$ [37], $LuFeO_3$ [38,39], and $SmFeO_3$ [40] thin-film heterostructures, where strain engineering at the interface between films and substrates plays a crucial role for emerging ferroelectricity. Recently, the contentious revelation of room-temperature FE order in $SmFeO_3$ crystal [28,29] has spurred investigations into elite members of the $RFeO_3$ series. A more recent observation has solidified this interest, confirming a FE order below ∼210 K, accompanied by a notable ME coupling along the c-axis in $HoFeO_3$ [31]. The varied sources of ferroelectricity in $RFeO_3$ compounds serve as a catalyst for further exploration into the multifaceted ferroic properties of the yet unexplored $TbFeO_3$. In contrast to previous observations of FE order across the entire series of the $RFeO_3$ family, two distinct FE orders are now observed along the c-axis in $TbFeO_3$ crystal. This observation sheds light on the FE behavior across the entirety of the $RFeO_3$ family. The current findings also emphasize an unprecedented observation of magnetostriction-driven ME coupling in the $TbFeO_3$ crystal, and they represent a unique example in chemically single-phase type-II multiferroics.

For orthoferrite $TbFeO_3$, the compound of our interest, the Fe^{3+} spins order antiferromagnetically in the G-type G_xF_z magnetic state at $T_N = 650$ K. Upon cooling, as a result of the Fe^{3+}-Tb^{3+} interaction, the Fe^{3+} spins reorient to order in the G_xF_x state from G_xF_z, and Tb^{3+} spins order in the $F_x'C_y'$ state at 8.5 K. However, below 3 K, another spin reorientation occurs, leading to a transition to a low-temperature (LT) phase. This transition causes the Fe^{3+} spins to revert back to their high-temperature (HT) G_xF_z state, while the Tb^{3+} spins order antiferromagnetically in the $A_x'G_y'$ state [41–44]. Incidentally, ferroelectric orderings at HT (200 K) and LT (3 K) are always coincident with the G-type G_xF_z magnetic state of the Fe sublattice. Moreover, below 3 K, ferroelectric ordering is further associated with the Tb spin ordering in $TbFeO_3$.

The $TbFeO_3$ single crystals were grown by the flux method [45]. Laboratory-based powder x-ray diffraction was conducted using a Bruker D8 x-ray diffractometer with monochromated Cu $K\alpha$ radiation (40.0 kV, 30.0 mA). Rietveld refinement was carried out using FULLPROF software. A single-crystal synchrotron diffraction study was performed at beamline P09/PETRA III at DESY, Germany [46]. The crystals were mounted in a He-flow magnet cryostat covering the temperature range from 2 to 300 K with the cryostat mounted on a horizontal Psi diffractometer. The experiment was conducted at photon energies significantly below the L2/3 absorption edges of the rare-earth elements to avoid fluorescence. Crystal was fixed firmly during all the magnetic-field-dependent experiments.

A single-crystal neutron diffraction study was performed on a neutron-sized crystal, which was glued on a vanadium pin and placed on the self-dedicated low-temperature Displex device [47]. A full data set was collected at 200 K at the D19 diffractometer (ILL, Grenoble) operating in high-resolution mode with a wavelength of 0.9482 Å. Data sets consist of omega scans at selected χ and ϕ positions to obtain a completeness above 90%. The data collection was performed using the NOMAD software from the ILL. The reflection data were indexed with the ILL program PFIND and integrated with the RETREAT software [48] from the ILL program suite. The correction for attenuation was carried out with the ILL program D19ABS [49].

Dielectric permittivity was recorded in an E4980A LCR meter (Agilent Technologies, USA) equipped with a PPMS-II system (Quantum Design, USA). The pyroelectric current was recorded using an electrometer (Keithley, model 6517B) at a constant temperature sweep rate. The P-E loops were recorded using a ferroelectric loop tracer (Radiant Technology, USA). All electrical contacts were fabricated using an air-drying silver paint. The dc magnetization was measured in a commercial magnetometer of Quantum Design (MPMS, evercool) both in zero-field-cooled (ZFC) and field-cooled (FC) protocols. For ZFC measurements, crystal was cooled in zero magnetic field, while measurements were carried out in the warming mode with a desired magnetic field (H). For the FC protocol, crystal was cooled in field, and measurements were carried out similar to the ZFC protocol. Raman measurements were carried out using a Horiba Labram HR Raman spectrometer (excitation wavelength = 532 nm with a spot size of 1 μm).

We refer to the Supplemental Material (SM) [50] (including Refs. [1,2] for reported Raman spectroscopy) for details on structural, magnetic characterization, pyroelectric results, magnetoelectric coupling, and starting with the dielectric permittivity (ϵ) results. The powder x-ray diffraction was performed at 300 K on powdered crystal, which is shown in Fig. S1 of the SM [50], where Rietveld refinement confirms the single chemical phase of $TbFeO_3$. The Raman spectrum is depicted in Fig. S2 of the SM [50], reproducing the previous reports [45,51]. Signatures of HT and LT ferroelectric orders were initially discerned through the ϵ measurements. The real (ϵ') components of ϵ at a frequency of 2 kHz are depicted with T in Figs. 1(a) and 1(d) for the HT and LT regions, respectively. A subtle anomaly is noticeable near ∼200 K, while an apparent peak is observed close to ∼4 K. The absence of a peak shift with frequency further indicates the onset of long-range polar order (see Fig. S3 of the SM [50] for details of ϵ results). The value of ϵ' at 2 K is significantly higher than the previous reports [6,45,52], which might be attributed to imperfection of the crystal. The result of bias electric field (BE) measurement further confirms polar order with an onset around 200 K (see Fig. S4 of the SM [50]). The pyroelectric current density (I_p) was recorded to further characterize polar order. The peaks in $I_p(T)$ are observed around ∼200 K and ∼3 K along the c-axis, as depicted in Figs. S5 and S6 of the SM [50] (see also Refs. [3–5] therein) for characterizing the genuine occurrence of $I_p(T)$ in the HT and LT regions, respectively [53–55]. Time-integrated $I_p(T)$ yields electric polarization (P). The variations of $P(T)$ are illustrated at ±5 kV/cm poling fields in Figs. 1(b) and 1(e) for the HT and LT regions, respectively. Reversal of P due to opposite poling fields corroborates the emergence of ferroelectric order below 200 (T_{FE1}) and 3 K (T_{FE2}) in $TbFeO_3$. Thermal variation of ZFC magnetization (M) recorded in the LT region with a

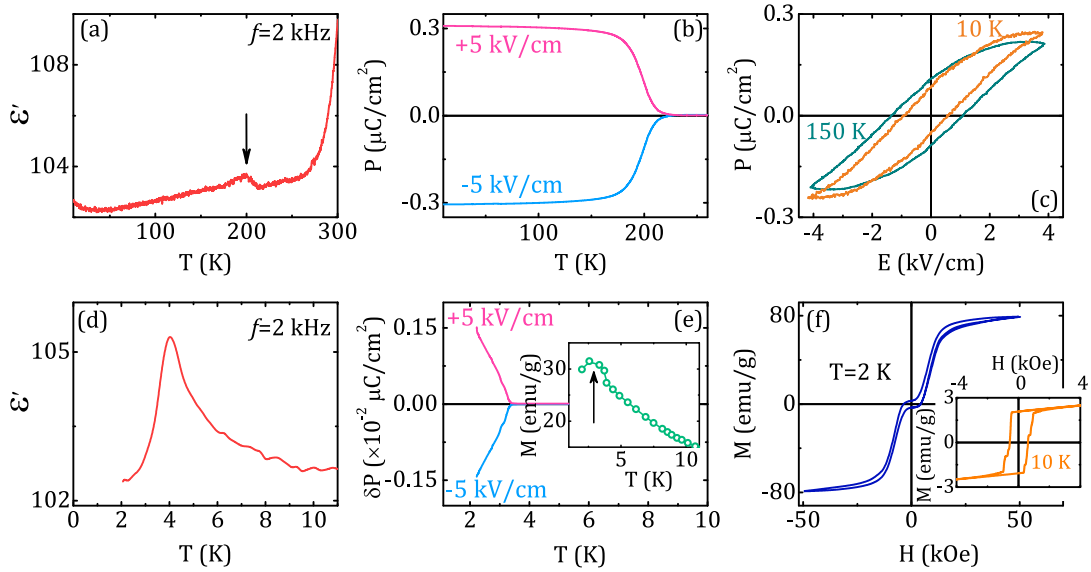

FIG. 1. Thermal variations of ϵ' in the (a) high-temperature (highlighting T_{FE1}) and (d) low-temperature regions; electric polarization (P) in the (b) high-temperature and (e) low-temperature regions. (c) P-E and (f) M-H loops at selected temperatures. Insets show (e) ZFC magnetization with T, highlighting T_{FE2}. (f) M-H loop at 10 K. All the measurements were recorded along the c-axis.

10 kOe magnetic field is depicted in the inset of Fig. 1(e). A maximum in $M(T)$ around T_{FE2} indicates a ME consequence. The $M(T)$ curve recorded in the ZFC protocol (Fig. S7 of the SM [50]) does not indicate any convincing signature around T_{FE1}.

Figure 1(c) displays the P versus E loops at selected temperatures below T_{FE1}, where E represents electric field applied along the c-axis. The $P(E)$ curve exhibits a saturating value of $P \sim 0.25$ μC/cm^2 at 10 K, closely matching that observed from pyroelectric measurement. Our attempts to measure P along the a and b axes consistently yielded negative results, aligning with observations of ferroelectricity along the c direction in orthoferrites such as $GdFeO_3$ [27], $DyFeO_3$ [30], and $HoFeO_3$ [31]. Figure 1(f) depicts M versus H curves with H applied along the c-axis at representative temperatures of 2 and 10 K [inset of Fig. 1(f)]. The loop at 10 K exhibits a square-type FM hysteresis, corroborating a weak FM moment along the c-axis [56]. The loop at 2 K exhibits a magnetic-field-induced transition around 7.5 kOe, as evident in the first-order derivative plot (Fig. S8 of the SM [50]).

To investigate the potential ME coupling, $I_p(T)$ curves were recorded under two H orientations, both $||$ and $\perp$ to the c-axis. Notably, results obtained with $H \perp c$-axis exhibited similar trends to those recorded for $H \,||\, c$, as illustrated in Fig. S9 of the SM [50]. The variations of $P(T)$, derived from the time integration of recorded $I_p(T)$, for HT and LT regions are presented in Figs. 2(a) and 2(d), respectively, for selected $H \,||\, c$-axis. The insets of the figures magnify the changes of $P(T)$. Notably, in both cases, the values of P exhibit nonmonotonic changes with H. The percentage of changes in P, defined as $\Delta P/P(\%) = [P(H)/P(0) - 1] \times 100$, at 180 (below T_{FE1}) and 2 K (below T_{FE2}), are plotted with H in Figs. 2(b) and 2(e), respectively. The variation of $\Delta P/P$ with H differs for applied H directions relative to the c-axis, indicating anisotropy in ME coupling (also refer to Fig. S9 of the SM [50]). For $H \,||\, c$, the $\Delta P/P(\%)$ at 180 K decreases with increasing H, reaching a minimum around 30 kOe, beyond which it increases slowly until 90 kOe. The maximum value of $|\Delta P/P|$ is ∼8% at $H = 30$ kOe. Conversely, below T_{FE2}, the $\Delta P/P(\%)$-value increases with H until ∼20 kOe, beyond which it shows a slowly decreasing trend. Intriguingly, the maximum $|\Delta P/P|$-value is substantial, reaching ∼38% at 2 K for $H = 20$ kOe. The variation P with H below T_{FE2} is consistent with the previous reports [57,58]. However, the $\Delta P/P(\%)$-value at 20 kOe diminishes at 2.5 K, following a similar dependence beyond 20 kOe (see Fig. S10 of the SM [50]).

Measurements of dynamic response of ME coupling was conducted at representative temperatures of 180 (below T_{FE1}) and 2 K (below T_{FE2}), as depicted in Figs. 2(c) and 2(f). The $H(t)$ was varied in between ±10 kOe over time (t) with a sweep-rate of 100 Oe/s. Distinctive features in the ME effects below T_{FE1} and T_{FE2} are noted, as manifested by the changes in I_P with t driven by $H(t)$. At 180 K, $I_P(t)$ exhibits continuous changes in response to $H(t)$. The time periods of $I_P(t)$ and $H(t)$ are found to be different, which has rarely been observed. Conversely at 2 K, $I_P(t)$ remains zero with variation in $H(t)$, except when $H(t)$ alters polarization direction. Nonzero I_P signals are observed just before and after the zero crossing of $H(t)$, as evident in Fig. 2(f). The characteristic signatures of I_P driven by the zero-crossing of $H(t)$ hold potential for sensor applications. However, this ME coupling gradually diminishes with increasing temperature, as shown in Fig. S11 of the SM [50].

To investigate structural distortion correlated with FE order, a synchrotron diffraction study [46] was conducted over a temperature range of 2–300 K. The 2θ scans were recorded around the (221) reflection at different temperatures. Variation of diffraction peaks with l-values at selected T around T_{FE1} are highlighted in Fig. 3(a), revealing a peak shift with T. Upon closer examination, a weak shoulder emerges on the right-hand side below T_{FE1} at 200 K. This shoulder, indicated

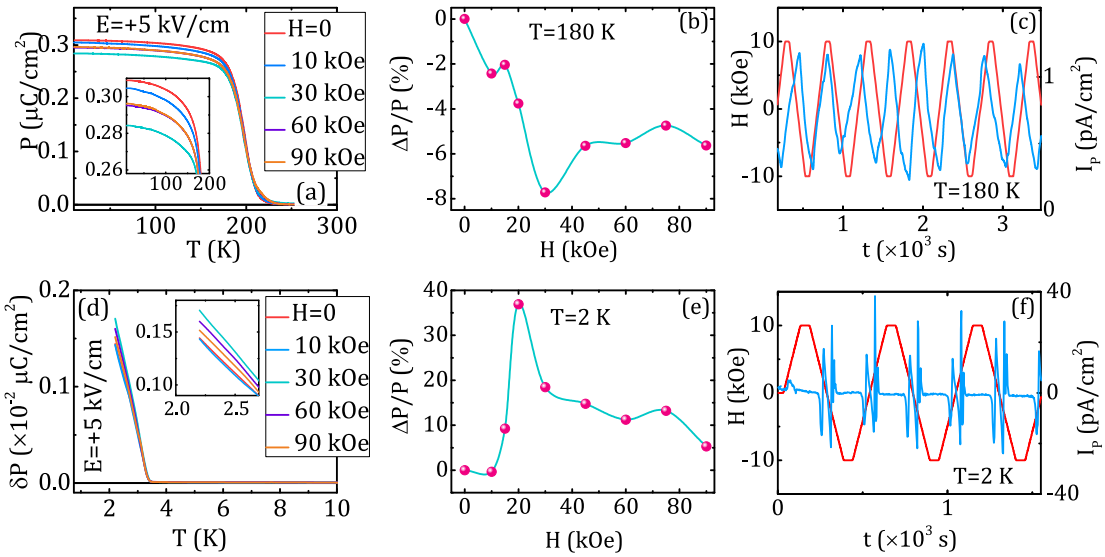

FIG. 2. Thermal variations of electric polarization (P) in the (a) high-temperature and (d) low-temperature regions recorded at selected magnetic fields (H). The variation of $\Delta P/P$ with H at (b) 180 and (e) 2 K; representative temperatures below high-temperature (T_{FE1}) and low-temperature (T_{FE2}) ferroelectric order. Time (t) profile of pyroelectric current (I_p) with H variations at (c) 180 and (f) 2 K, indicating the nature of magnetoelectric coupling. All the measurements were recorded along the c-axis.

by the arrows, shifts towards the main peak as temperature decreases, suggesting a possible structural distortion or transition associated with the FE order. Integrated intensities and peak shift are depicted with T in Figs. S12 and S13(a) of the SM [50], respectively. The peak shift correlates with the lattice constant, as the change in l-value in (22l) is inversely proportional to the lattice constant c. Thermal variation of $c/c(300\ \mathrm{K})$, where $c(300\ \mathrm{K})$ represents the c-value at 300 K, is depicted in Fig. 3(b). To investigate a possible structural correlation with the observed variation of P with H, we recorded

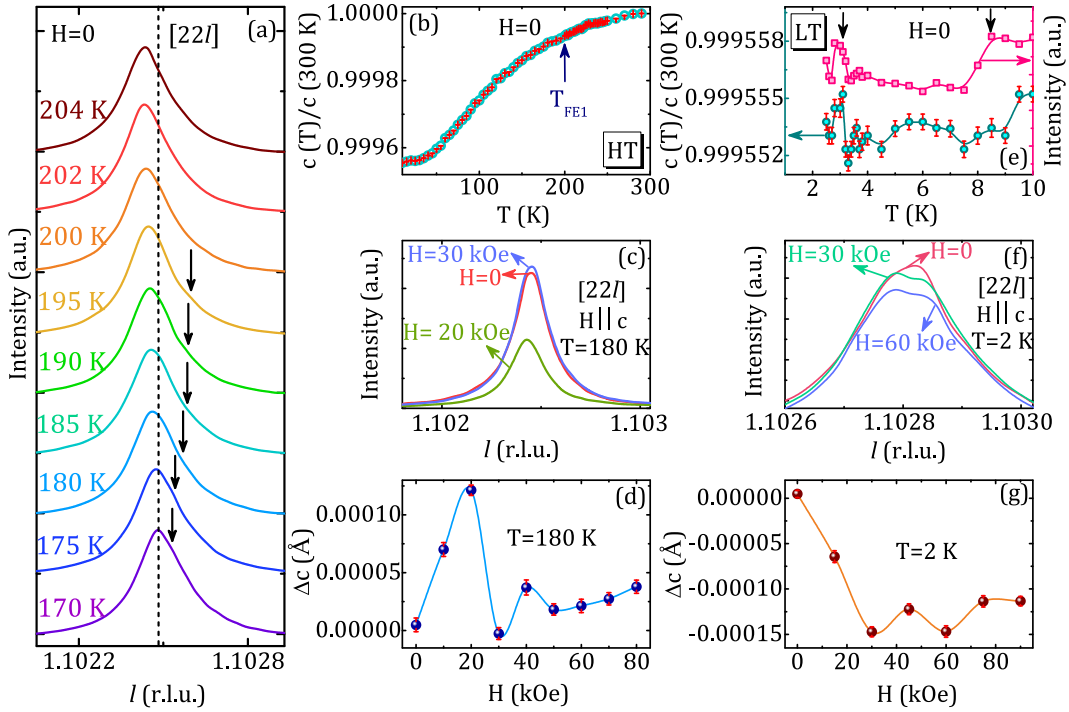

FIG. 3. (a) The l variation around (221) diffraction peaks at selected temperatures (T) in zero field, arrows highlighting the shoulder and broken vertical straight line guiding the peak shift with T. The T profile of the lattice constant scaled by the same at 300 K [$c(T)/c(300\ \mathrm{K})$] in (b) HT region and (e) LT region (left axis). (e) (right axis) T variation of integrated intensities of (22l) diffraction peak in LT region at $H = 0$. The l variation near (221) diffraction peaks at (c) 180 K and (f) 2 K at selected magnetic fields (H). Variation of Δc with H at (d) 180 K and (g) 2 K. Magnetic field was applied along the c-axis.

(22l) scans at 180 K for selected H along the c-axis, which are shown in Fig. 3(c). A significant suppression of the intensity of the diffraction peak is evident for H at 20 kOe. The variations in peak positions with respect to H exhibit a similar trend, as depicted in Fig. S13(b) of the SM [50]. This variation in peak position eventually indicates c lattice distortions, as depicted by the change in c (Δc) with H in Fig. 3(d), suggesting a maximum magnetostriction around 20 kOe. Although measurements with small increments in H would provide more precise magnetostriction results, the findings suggest that magnetostriction is correlated with the ME effects at 180 K. The variations in $\Delta P/P$, along with those in $\Delta c/c$ as a function of H, are compared in Fig. S10(a) of the SM [50].

Synchrotron diffraction study was further extended to LT regions around T_{FE2}. The scans along [22l] are shown in Fig. S14(a) of the SM [50] for selected temperatures around T_{FE2}. The integrated intensities (right axis) and $C(T)/c(300\ \text{K})$ (left axis) [obtained from peak shifts given in Fig. S14(b) of the SM [50]] are plotted with T in Fig. 3(e), revealing abrupt changes in $c(T)$ near 3 and 8.5 K, as indicated by the arrows. Incidentally, 3d-4f interaction driven Fe^{3+} and Tb^{3+} spin reorientation transitions occur at 8.5 and 3 K, respectively, suggesting significant magnetoelastic coupling. Moreover, the structural distortion at 3 K is associated with the LT FE order. The diffraction peaks were recorded with selected H at various T, as summarized in Fig. 3(f) and Figs. 15(a-d) of the SM [50]. The change in structure of the peak with H is significant at 2 K, compared to the results above 2 K, and it indicates significant involvement of magnetic domain-wall movements. The asymmetric diffraction peak was deconvoluted into two peaks, as demonstrated in Fig. S16 of the SM [50]. The variation of Δc with H, as obtained from the high-l peak shift, is shown in Fig. 3(g). The lattice contracts with increasing H until 30 kOe, beyond which it exhibits nonmonotonous behavior, analogous to that observed at 180 K. Below 30 kOe, the results indicate that an increase or decrease in P is associated with a corresponding decrease or increase in c under an applied magnetic field at 180 and 2 K, which are representative temperatures below T_{FE1} and T_{FE2}, respectively. The findings indicate a correlation between the ME effect and magnetostriction. The magnetostriction is significant at 2 K and decreases significantly above 2 K (see Figs. S15(e-h) of the SM [50]). The decrease in magnetostriction is correlated with the decreased ME consequence with increasing temperature.

At room temperature, $TbFeO_3$ crystalizes in the Shubnikov $Pbnm$ group [41,59,60], which precludes ferroelectricity. The structural and magnetic refinement of neutron diffraction was carried out using "modes" to identify the mode responsible for ferroelectricity, while assessing the amplitude values within the refinement error. To obtain a Shubnikov space group compatible with ferroelectricity, we analyzed all the possible subgroups using the ISODISTORT platform [61]. Our careful observations suggest that among all possible subgroups, the subgroup having the highest symmetry is $Pn'a'2_1$, allowing polarization along the c-axis. There are two structural irreducible representations needed to distort the parent $Pbnm$ structure into $Pna2_1$. The application of an extra magnetic irreducible representation yields the final $Pn'a'2_1$ Shubnikov

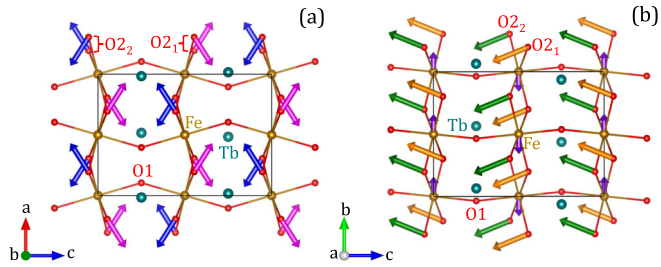

FIG. 4. (a) Active modes for Γ^{1+} representation at 200 K. The pink and blue arrows are the results of two different vector modes acting on $O2_1$ and $O2_2$, respectively. (b) Active modes for Γ^{4-} representation at 200 K. The violet, orange, and green arrows correspond with the displacement of the Fe, $O2_1$, and $O2_2$ atoms, respectively.

space group. Here, we discuss only Γ^{4-} and Γ^{1+}, because they are the only displacement modes. Within this Shubnikov group, there are 15 possible mode vectors acting on the nuclear part at 200 K, with only six modes being active for refinement using the $Pn'a'2_1$ space group. The values of 15 amplitude modes, acting on different atoms of $TbFeO_3$, are listed in Table I of the SM [50].

Figures 4(a) and 4(b) depict two structural irreducible representations for Γ^{1+} and Γ^{4-}, respectively. Γ^{4-} acts on all atoms, whereas Γ^{1+} influences Tb and O atoms. Moreover, the global amplitude of each representation is 0.108(8) Å for Γ^{4-} and 0.0065(18) Å for Γ^{1+}, indicating that the distortions produced by Γ^{1+} representation are practically negligible. Among two active modes of Γ^{1+}, A14 and A15 amplitudes act on $O2_1$ and $O2_2$ atoms, denoted by the pink and blue arrows in Fig. 4(a), respectively. However, these amplitudes preclude ferroelectricity, since the displacements of $O2_1$ and $O2_2$ atoms are compensated by identical displacements in opposite directions. A similar behavior is observed for Fe atoms. Out of four active modes of Γ^{4-}, only A2 acts on Fe atoms. However, this cannot explain ferroelectricity, as the amplitude of this mode is null within the unit cell. The distortions of Fe atoms are represented by violet arrows in Fig. 4(b).

The remaining three active modes of Γ^{4-}, namely A6, A7, and A8, act on $O2_1$ and $O2_2$ atoms, forming connections between Fe atoms in the ab plane. The displacements of $O2_1$ and $O2_2$ atoms are illustrated by orange and green arrows, respectively, in Fig. 4(b). The components of these displacements produce a net distortion of $O2_1$ and $O2_2$ atoms along the c-axis in the $TbFeO_3$ unit cell. However, these modes represent a component along the a axis, and they cancel each other out. Here, the values of the amplitudes are 0.050(9) Å for A6(Γ^{4-}), −0.089(8) Å for A7(Γ^{4-}), and −0.034(9) Å for A8(Γ^{4-}), as listed in Table I. All these amplitudes are significantly larger than their error and produce a net polarization along the c-axis. Therefore, based on amplitude refinement, the global distortions of $O2_1$ and $O2_2$ in the $Pna2_1$ structure permit ferroelectricity along the c-axis in $TbFeO_3$. Using the atomic displacements, we obtain an estimate of P to be ∼3.5 μC/cm^2 using a simplified formula, $P = 1/V[\sum_i(m_i\Delta z_i Z_i)e]$, where m_i is the crystallographic site multiplicity, Δz_i is the displacement along the polar axis (here, crystallographic c-axis), $Z_i e$ is the charge, and V is the unit-cell volume. This calculated value of P is ∼10 times higher than the experimental P-value.

Instead of a point-charge model, the Berry phase method using a first-principles calculation would provide a more realistic P-value [62].

In the HT region, the iron sublattice orders antiferromagnetically, accompanied by a weak Dzyaloshinskii-Moriya (DM) interaction-induced ferromagnetic moment [44,63,64]. The neutron results do not indicate any convincing signature of a modification in the iron spin direction around T_{FE1}. However, low-temperature Raman studies, as well as Tb oscillations, reported an interesting observation regarding magnetoelastic coupling driven by the crosstalk between Tb and Fe spins [65]. Adopting a two-sublattice model of the four Fe^{3+} moments in each unit cell of $TbFeO_3$, two doubly degenerate spin-wave branches (M_1 and M_2) were proposed for the iron sublattices [51]. Thermal variations of M_1 and M_2 magnons indicate a change of slope near T_{FE1}, driven by a proposed exchange striction mechanism. Thermal variation of Raman spectra further indicates the emergence of a new mode around 430 cm^{-1} close to FE ordering temperature, suggesting a structural transition [65]. Consistent with the above results, current synchrotron diffraction results suggest a structural transition, where a net displacement of $O2_1$ and $O2_2$ atoms in the $Pn'a'2_1$ Shubnikov space group reveals a ferroelectric polarization along the c-axis. The observation of another ferroelectric order at T_{FE2} is consistent with that reported in orthoferrites [27,30]. As suggested in $GdFeO_3$ [27] and $DyFeO_3$ [30], the ferroelectric order at low temperature is associated with coexisting Tb and Fe spin order in $TbFeO_3$ [44]. Finally, the results reveal two distinct ferroelectric orders at T_{FE1} and T_{FE2}, each with different origins of ferroelectricity. The ferroelectric order at LT close to rare ordering has been observed in $GdFeO_3$ [27] and $DyFeO_3$ [30] without any evidence of HT ferroelectric order, associated with the $3d$ moment ordering. On the other hand, the HT ferroelectric order has been proposed for $HoFeO_3$ without LT ferroelectric ordering [31]. $TbFeO_3$, however, exhibits the unique characteristic of both LT and HT ferroelectric order within the entire $RFeO_3$ family. The ME coupling and ferroelectricity in $TbFeO_3$ have been proposed based on symmetry calculations [66]. Moreover, ME coupling has also been proposed in other ferrites [67].

The variation of P with H, indicative of ME coupling, exhibits a nonmonotonous behavior in our observations. When a magnetic field is applied along the c-axis, distinct minima and maxima are observed in the P-H curves below HT and LT ferroelectric orders, respectively. Below the HT ferroelectric order, the minimum occurs at a level nearly six times higher than the coercivity, suggesting that magnetic anisotropy does not play a leading role in ME coupling. Instead, magnetostriction emerges as a more influential factor, evidenced by significant distortion along the c-axis under the influence of H. The connection between magnetostriction and ME coupling has seldom been explored in chemically single-phase compounds [68,69], unlike in composites [70] and films [71,72]. Below LT ferroelectric order, the scenario differs. The $P(H)$ starts to increase above $\sim$10 kOe, with a maximum around 20 kOe, nearly twice the coercivity at 2 K. This result may be influenced by the magnetic-field-induced change in magnetic structure around 5 kOe at 2 K [44]. However, the additional impact of magnetostriction is rather more influential on ME coupling [Fig. 3(g)]. The direct observation of intrinsic magnetostriction-driven ME coupling is a rare consequence, particularly in a chemically single-phase compound.

To conclude, our investigation reveals two distinct ferroelectric orders, occurring at around 200 and 2 K, respectively, in $TbFeO_3$, indicating a type-II multiferroic behavior. This result contributes to resolving the controversy surrounding the emergence of ferroelectric order in the $RFeO_3$ family. Synchrotron and neutron diffraction results confirm a structural distortion to a polar $Pna2_1$ structure, correlated with the emergence of ferroelectricity below 200 K. Specifically, the net distortion of oxygen displacements along the c-axis ($O2_1$ and $O2_2$) engineers ferroelectric order. Additionally, the Tb spin order below 3 K involves ferroelectric order. The polarization value undergoes a significant change upon application of magnetic fields along the c-axis. This change is accompanied by a notable lattice distortion, suggesting a magnetostriction-driven magnetoelectric coupling. Our findings represent a substantial contribution to advancing the understanding of magnetoelectric coupling in type-II multiferroics, particularly those operating at higher temperature, with significant ferroelectric polarization, and boasting commendable magnetoelectric coupling.

S.G. acknowledges the financial support from SERB, Government of India (Project No. CRG/2022/000718), and BRNS, Government of India (Project No. 58/14/09/2023/11737). Financial support by the Department of Science & Technology, Government of India (Project No. I-20140424), provided within the framework of the India@DESY collaboration, is gratefully acknowledged for the synchrotron diffraction experiment at DESY, Germany. A.I. acknowledges the financial support from SERB, Government of India (Project No. SPG/2021/002397). The authors also acknowledge the ILL for the allocated beam time (doi:10.5291/ILL-DATA.5-11-438).

[1] W. C. Röntgen, About the electrodynamic force caused by the movement of a dielectric in a homogeneous electric field, Ann. Phys. (NY) **35**, 264 (1888).

[2] P. Curie, On symmetry in physical phenomena, symmetry of an electric field and a magnetic field, J. Phys. Theor. Appl. **3**, 393 (1894).

[3] N. A. Spaldin, S.-W. Cheong, and R. Ramesh, Multiferroics: Past, present, and future, Phys. Today **63** (10), 38 (2010).

[4] M. Fiebig, Revival of the magnetoelectric effect, J. Phys. D **38**, R123 (2005).

[5] S. W. Cheong, and M. Mostovoy, Multiferroics: a magnetic twist for ferroelectricity, Nat. Mater. **6**, 13 (2007).

[6] T. Kimura, T. Goto, H. Shintani, K. Ishizaka, T. Arima, and Y. Tokura, Magnetic control of ferroelectric polarization, Nature (London) **426**, 55 (2003).

[7] T. Kimura, Spiral magnets as magnetoelectrics, Annu. Rev. Mater. Res. **37**, 387 (2007).

[8] V. Laukhin, V. Skumryev, X. Martí, D. Hrabovsky, F. Sánchez, M. V. García-Cuenca, C. Ferrater, M. Varela, U. Lüders, J. F. Bobo, and J. Fontcuberta, Electric-field control of exchange

bias in multiferroic epitaxial heterostructures, Phys. Rev. Lett. **97**, 227201 (2006).

[9] D. Yu, Y. Ga, J. Liang, C. Jia, and H. Yang, Voltage-controlled Dzyaloshinskii-Moriya interaction torque switching of perpendicular magnetization, Phys. Rev. Lett. **130**, 056701 (2023).

[10] J. T. Heron, M. Trassin, K. Ashraf, M. Gajek, Q. He, S. Y. Yang, D. E. Nikonov, Y.-H. Chu, S. Salahuddin, and R. Ramesh, Electric-field-induced magnetization reversal in a ferromagnet-multiferroic heterostructure, Phys. Rev. Lett. **107**, 217202 (2011).

[11] H. Béa, M. Gajek, M. Bibes, and A. Barthélémy, Spintronics with multiferroics, J. Phys.: Condens. Matter **20**, 434221 (2008).

[12] R. de Sousa, Multiferroics are a spintronics game changer, Physics **15**, 124 (2022).

[13] Y.-H. Chu, L. W. Martin, M. B. Holcomb, M. Gajek, S.-J. Han, Q. He, N. Balke, C.-H. Yang, D. Lee, W. Hu, Q. Zhan, P.-L. Yang, A. F. Rodríguez, A. Scholl, S. X. Wang, and R. Ramesh, Electric-field control of local ferromagnetism using a magnetoelectric multiferroic, Nat. Mater. **7**, 478 (2008).

[14] J. F. Scott, Multiferroic memories, Nat. Mater. **6**, 256 (2007).

[15] M. Gajek, M. Bibes, S. Fusil, K. Bouzehouane, J. Fontcuberta, A. Barthélémy, and A. Fert, Tunnel junctions with multiferroic barriers, Nat. Mater. **6**, 296 (2007).

[16] J. C. Chen, G. Bhave, F. Alrashdan, A. Dhuliyawalla, K. J. Hogan, A. G. Mikos, and J. T. Robinson, Self-rectifying magnetoelectric metamaterials for remote neural stimulation and motor function restoration, Nat. Mater. **23**, 139 (2024).

[17] J. Wang, J. B. Neaton, H. Zheng, V. Nagarajan, S. B. Ogale, B. Liu, D. Viehland, V. Vaithyanathan, D. G. Schlom, U. V. Waghmare, N. A. Spaldin, K. M. Rabe, M. Wuttig, and R. Ramesh, Epitaxial $BiFeO_3$ multiferroic thin film heterostructures, Science **299**, 1719 (2003).

[18] R. O. Cherifi, V. Ivanovskaya, L. C. Phillips, A. Zobelli, I. C. Infante, E. Jacquet, V. Garcia, S. Fusil, P. R. Briddon, N. Guiblin, A. Mougin, A. A. Ünal, F. Kronast, S. Valencia, B. Dkhil, A. Barthélémy, and M. Bibes, Electric-field control of magnetic order above room temperature, Nat. Mater. **13**, 345 (2014).

[19] T. Kimura, Y. Sekio, H. Nakamura, T. Siegrist, and A. P. Ramirez, Cupric oxide as an induced-multiferroic with high-T_C, Nat. Mater. **7**, 291 (2008).

[20] M. Soda, T. Ishikura, H. Nakamura, Y. Wakabayashi, and T. Kimura, Magnetic ordering in relation to the room-temperature magnetoelectric effect of $Sr_3Co_2Fe_{24}O_{41}$, Phys. Rev. Lett. **106**, 087201 (2011).

[21] B. Kundys, A. Maignan, and Ch. Simon, Multiferroicity with high-T_C in ceramics of the $YBaCuFeO_5$ ordered perovskite, Appl. Phys. Lett. **94**, 072506 (2009).

[22] S.-N. Dong, Y.-P. Yao, J.-Q. Li, Y.-J. Song, Y.-K. Liu, and X.-G. Li, Room temperature multiferroicity in $Bi_{4.2}K_{0.8}Fe_2O_{9+\delta}$, Sci. Rep. **3**, 1245 (2013).

[23] F. Orlandi, D. Delmonte, G. Calestani, E. Cavalli, E. Gilioli, V. V. Shvartsman, P. Graziosi, S. Rampino, G. Spaggiari, C. Liu, W. Ren, S. Picozzi, M. Solzi, M. Casappa, and F. Mezzadri, γ-$BaFe_2O_4$: a fresh playground for room temperature multiferroicity, Nat. Commun. **13**, 7968 (2022).

[24] S. J. Yuan, W. Ren, F. Hong, Y. B. Wang, J. C. Zhang, L. Bellaiche, S. X. Cao, and G. Cao, Spin switching and magnetization reversal in single-crystal $NdFeO_3$, Phys. Rev. B **87**, 184405 (2013).

[25] Z. Y. Zhao, X. Zhao, H. D. Zhou, F. B. Zhang, Q. J. Li, C. Fan, X. F. Sun, and X. G. Li, Ground state and magnetic phase transitions of orthoferrite $DyFeO_3$, Phys. Rev. B **89**, 224405 (2014).

[26] T. N. Stanislavchuk, Y. Wang, Y. Janssen, G. L. Carr, S.-W. Cheong, and A. A. Sirenko, Magnon and electromagnon excitations in multiferroic $DyFeO_3$, Phys. Rev. B **93**, 094403 (2016).

[27] Y. Tokunaga, N. Furukawa, H. Sakai, Y. Taguchi, T.-H. Arima, and Y. Tokura, Composite domain walls in a multiferroic perovskite ferrite, Nat. Mater. **8**, 558 (2009).

[28] J.-H. Lee, Y. K. Jeong, J. H. Park, M.-A. Oak, H. M. Jang, J. Y. Son, and J. F. Scott, Spin-canting-induced improper ferroelectricity and spontaneous magnetization reversal in $SmFeO_3$, Phys. Rev. Lett. **107**, 117201 (2011).

[29] C.-Y. Kuo, Y. Drees, M. T. Fernández-Díaz, L. Zhao, L. Vasylechko, D. Sheptyakov, A. M. T. Bell, T. W. Pi, and H.-J. Lin, $k = 0$ Magnetic structure and absence of ferroelectricity in $SmFeO_3$, Phys. Rev. Lett. **113**, 217203 (2014).

[30] Y. Tokunaga, S. Iguchi, T. Arima, and Y. Tokura, Magnetic-field-induced ferroelectric state in $DyFeO_3$, Phys. Rev. Lett. **101**, 097205 (2008).

[31] K. Dey, A. Indra, S. Mukherjee, S. Majumdar, J. Strempfer, O. Fabelo, E. Mossou, T. Chatterji, and S. Giri, Natural ferroelectric order near ambient temperature in the orthoferrite $HoFeO_3$, Phys. Rev. B **100**, 214432 (2019).

[32] R. L. White, Review of recent work on the magnetic and spectroscopic properties of the rare-earth orthoferrite, J. Appl. Phys. **40**, 1061 (1969).

[33] M. Eibschütz, S. Shtrikman, and D. Treves, Mössbauer studies of ^{57}Fe in orthoferrites, Phys. Rev. **156**, 562 (1967).

[34] Z. Y. Zhao, X. M. Wang, C. Fan, W. Tao, X. G. Liu, W. P. Ke, F. B. Zhang, X. Zhao, and X. F. Sun, Magnetic phase transitions and magnetoelectric coupling of $GdFeO_3$ single crystals probed by low-temperature heat transport, Phys. Rev. B **83**, 014414 (2011).

[35] A. Stroppa, M. Marsman, G. Kresse, and S. Picozzi, The multiferroic phase of $DyFeO_3$: an *ab initio* study, New J. Phys. **12**, 093026 (2010).

[36] Y. K. Jeong, J.-H. Lee, S.-J. Ahn, S.-W. Song, H. M. Jang, H. Choi, and J. F. Scott, Structurally tailored hexagonal ferroelectricity and multiferroism in epitaxial $YbFeO_3$ thin-film heterostructures, J. Am. Chem. Soc. **134**, 1450 (2012).

[37] S. Mukherjee, A. Roy, S. Auluck, R. Prasad, R. Gupta, and A. Garg, Room temperature nanoscale ferroelectricity in magnetoelectric $GaFeO_3$ epitaxial thin films, Phys. Rev. Lett. **111**, 087601 (2013).

[38] Y. K. Jeong, J.-H. Lee, S.-J. Ahn, and H. M. Jang, Epitaxially constrained hexagonal ferroelectricity and canted triangular spin order in $LuFeO_3$ thin films, Chem. Mater. **24**, 2426 (2012).

[39] U. Chowdhury, S. Goswami, D. Bhattacharya, J. Ghosh, S. Basu, and S. Neogi, Room temperature multiferroicity in orthorhombic $LuFeO_3$, Appl. Phys. Lett. **105**, 052911 (2014).

[40] Z. Cheng, F. Hong, Y. Wang, K. Ozawa, H. Fujii, H. Kimura, Y. Du, X. Wang, and S. Dou, Interface strain-induced multiferroicity in a $SmFeO_3$ Film, ACS Appl. Mater. Interfaces **6**, 7356 (2014).

[41] J. E. Bouree and J. Hammann, Experimental demonstration of shape effects in terbium orthoferrite, J. Phys. **36**, 391 (1975).

[42] K. P. Belov, A. K. Zvezdin, and A. A. Mukhin, Magnetic phase transitions in terbium orthoferrite, Sov. Phys. JETP **49**, 557 (1979).

[43] S. A. Guretskii, A. P. Ges, A. M. Luginets, A. S. Milovanov, V. D. Fil, and S. V. Zherlitsyn, Low-temperature magnetic properties of terbium orthoferrite single crystals, Cryst. Res. Technol. **31**, 897 (1996).

[44] S. Artyukhin, M. Mostovoy, N. P. Jensen, D. Le, K. Prokes, V. G. de Paula, H. N Bordallo, A. Maljuk, S. Landsgesell, H. Ryll *et al.*, Solitonic lattice and Yukawa forces in the rare-earth orthoferrite $TbFeO_3$, Nat. Mater. **11**, 694 (2012).

[45] R. M. Dubrovin, E. M. Roginskii, V. A. Chernyshev, N. N. Novikova, M. A. Elistratova, I. A. Eliseyev, A. N. Smirnov, A. I. Brulev, K. N. Boldyrev, V. Yu. Davydov, R. V. Mikhaylovskiy, A. M. Kalashnikova, and R. V. Pisarev, Lattice dynamics and mixing of polar phonons in the rare-earth orthoferrite $TbFeO_3$, Phys. Rev. B **110**, 134310 (2024).

[46] J. Strempfer, S. Francoual, D. Reuther, D. K. Shukla, A. Skaugen, H. Schulte-Schrepping, T. Kracht, and H. Franz, Resonant scattering and diffraction beamline P09 at PETRA III, J. Synch. Radiat. **20**, 541 (2013).

[47] J. Archer and M. S. Lehmann, A simple adjustable mount for a two-stage cryorefrigerator on an Eulerian cradle, J. Appl. Crystallogr. **19**, 456 (1986).

[48] G. J. McIntyre and R. F. D. Stansfield, A general Lorentz correction for single-crystal diffractometers, Acta Crystallogr. Sect. A **44**, 257 (1988).

[49] J. C. Matthewman, P. Thompson, and P. J. Brown, The Cambridge crystallography subroutine library, J. Appl. Crystallogr. **15**, 167 (1982).

[50] See Supplemental Material at http://link.aps.org/supplemental/10.1103/PhysRevB.111.L140412 for details on Raman spectroscopy, structural, dielectric permittivity, magnetic characterization, pyroelectric results, magnetoelectric coupling, and analysis of the neutron diffraction results.

[51] S. Venugopalan, M. Dutta, A. K. Ramdas, and J. P. Remeika, Magnetic and vibrational excitations in rare-earth orthoferrites: A Raman scattering study, Phys. Rev. B **31**, 1490 (1985).

[52] G. A. Komandin, A. M. Kuzmenko, I. E. Spektor, and A. A. Mukhin, Electric-dipole and magnetic absorption in $TbFeO_3$ single crystals in the THz–IR range, J. Appl. Phys. **133**, 194101 (2023).

[53] N. Terada, Y. S. Glazkova, and A. A. Belik, Differentiation between ferroelectricity and thermally stimulated current in pyrocurrent measurements of multiferroic $M Mn_7O_{12}$ (M = Ca, Sr, Cd, Pb), Phys. Rev. B **93**, 155127 (2016).

[54] T. N. M. Ngo, U. Adem, and T. T. M. Palstra, The origin of thermally stimulated depolarization currents in multiferroic $CuCrO_2$, Appl. Phys. Lett. **106**, 152904 (2015).

[55] W. Liu and C. A. Randall, Thermally stimulated relaxation in Fe-doped $SrTiO_3$ systems: I. single crystals, J. Am. Ceram. Soc. **91**, 3245 (2008).

[56] D. Treves, Studies on Orthoferrites at the Weizmann Institute of Science, J. Appl. Phys. **36**, 1033 (1965).

[57] V. Yu. Ivanov, A. M. Kuzmenko, A. Yu. Tikhanovskii, and A. A. Mukhin, Metamagnetic and orientational transitions in $TbFeO_3$ orthoferrite: magnetoelectric phase diagrams, Eur. Phys. J. Plus **138**, 818 (2023).

[58] V. Yu. Ivanov, A. M. Kuzmenko, A. Yu. Tikhanovskii, A. A. Pronin, and A. A. Mukhin, Observation of magnetic-field-induced electric polarization in terbium orthoferrite, JETP Lett. **117**, 38 (2023).

[59] E. F. Bertaut, J. Chappert, J. Mareschal, J. P. Rebouillat, and J. Sivardiére, Structures magnetiques de $TbFeO_3$, Solid State Commun. **5**, 293 (1967).

[60] J. Tejada, X. X. Zhang, A. Roig, O. Nikolov, and E. Molins, Quantum tunneling of antiferromagnetic domain walls in $TbFeO_3$ single crystal, Europhys. Lett. **30**, 227 (1995).

[61] B. J. Campbell, H. T. Stokes, D. E. Tanner, and D. M. Hatch, *ISODISPLACE*: a web-based tool for exploring structural distortions, J. Appl. Crystallogr. **39**, 607 (2006).

[62] M. V. Berry, Quantal phase factors accompanying adiabatic changes, Proc. R. Soc. London Ser. A **392**, 45 (1984).

[63] A. K. Ovsianikov, O. V. Usmanov, I. A. Zobkalo, W. Schmidt, A. Maity, V. Hutanu, E. Ressouche, K. A. Shaykhutdinov, K. Yu Terentjev, S. V. Semenov, M. Meven, G. Roth, and L. Peters, Inelastic neutron studies and diffraction in magnetic fields of $TbFeO_3$ and $YbFeO_3$, J. Magn. Magn. Mater. **563**, 170025 (2022).

[64] S. A. Skorobogatov, K. A. Shaykhutdinov, D. A. Balaev, M. S. Pavlovskii, A. A. Krasikov, and K. Yu. Terentjev, Spin dynamics and exchange interaction in orthoferrite $TbFeO_3$ with non-Kramers rare-earth ion, Phys. Rev. B **106**, 184404 (2022).

[65] R. Vilarinho, M. C. Weber, M. Guennou, A. C. Miranda, C. Dias, P. Tavares, J. Kreisel, A. Almeida, and J. A. Moreira, Magnetostructural coupling in $RFeO_3$ (R = Nd, Tb, Eu and Gd), Sci. Rep. **12**, 9697 (2022).

[66] A. K. Zvezdin and A. A. Mukhin, Magnetoelectric interactions and phase transitions in a new class of multiferroics with improper electric polarization, JETP Lett. **88**, 505 (2008).

[67] B. Kundys, A. Maignan, D. Pelloquin, and Ch. Simon, Magnetoelectric interactions in polycrystalline multiferroic antiferromagnets $CuFe_{1-x}Rh_xO_2$ ($x = 0.00$ and $x = 0.05$), Solid State Sci. **11**, 1035 (2009).

[68] A. Gauzzi, G. Rousse, F. Mezzadri, G. L. Calestani, G. André, F. Bourée, M. Calicchio, E. Gilioli, R. Cabassi, F. Bolzoni *et al.*, Magnetoelectric coupling driven by inverse magnetostriction in multiferroic $BiMn_3Mn_4O_{12}$, J. Appl. Phys. **113**, 043920 (2013).

[69] M.-R. Li, E. E. McCabe, P. W. Stephens, M. Croft, L. Collins, S. V. Kalinin, Z. Deng, M. Retuerto, A. S. Gupta, H. Padmanabhan *et al.*, Magnetostriction-polarization coupling in multiferroic Mn_2MnWO_6, Nat. Commun. **8**, 2037 (2017).

[70] A. Aubert, V. Loyau, Y. Pascal, F. Mazaleyrat, and M. LoBue, Dynamic magnetostriction of $CoFe_2O_4$ and its role in magnetoelectric composites, Phys. Rev. Appl. **9**, 044035 (2018).

[71] J. Ma, J. Hu, Z. Li, and C.-W. Nan, Recent progress in multiferroic magnetoelectric composites: from bulk to thin films, Adv. Mater. **23**, 1062 (2011).

[72] H. Palneedi, D. Maurya, G.-Y. Kim, V. Annapureddy, M.-S. Noh, C.-Y. Kang, J.-W. Kim, J.-J. Choi, S.-Y. Choi, S.-Y. Chung *et al.*, Unleashing the full potential of magnetoelectric coupling in film heterostructures, Adv. Mater. **29**, 1605688 (2017).